GLOBAL BIOGEOCHEMICAL CYCLES, VOL. 14, NO. 3, PAGES 979-994, SEPTEMBER 2000

Global relationships of total inorganic carbon with temperature and nitrate in surface seawater

Kitack Lee,[1,2] Rik Wanninkhof,[2] Richard A. Feely,[3] Frank J. Millero,[4] and Tsung-Hung Peng[2]

Abstract. High quality total inorganic carbon (C_T) measurements made in the major ocean basins as part of the Joint Global Ocean Flux Study (JGOFS), the National Oceanic and Atmospheric Administration/Ocean Atmosphere Carbon Exchange Study (NOAA/OACES), and the Department of Energy/World Ocean Circulation Experiment (DOE/WOCE) programs are related to sea surface temperature (SST) and nitrate (NO_3^-). A simple two-parameter function with SST and NO_3^- of the form $NC_T = a + b\ SST + c\ SST^2 + d\ NO_3$ fits salinity (S)-normalized surface C_T ($NC_T = C_T \times 35/S$) data for different parts of the oceans within an area-weighted error of ±7 μmol kg^{-1} (1σ). Estimated values of NC_T using the derived algorithms with NO_3^- and SST are compared with values calculated from the surface partial pressure of CO_2 (pCO_{2SW}) [*Takahashi et al.*, 1997] and total alkalinity (A_T) [*Millero et al.*, 1998] fields using thermodynamic models. Comparisons of the estimated values of NC_T with measurements not used to derive the same algorithms, and comparisons with the values calculated from global A_T and pCO_{2SW} fields, give a realistic uncertainty of ±15 μmol kg^{-1} in estimated C_T. The derived correlations of NC_T with SST and NO_3^- presented here make it possible to estimate surface C_T over the ocean from climatological SST, S, and NO_3^- fields.

1. Introduction

The distribution of total inorganic carbon (C_T) in the upper ocean is primarily controlled by the factors that govern salinity. Other nonconservative processes, including precipitation and dissolution of calcium carbonate, photosynthesis, oxidation of organic matter, and the air-sea exchange of carbon dioxide (CO_2), also contribute to the large variability in the surface C_T concentration [*Chen and Pytkowicz*, 1979; *Takahashi et al.*, 1993; *Wanninkhof and Feely*, 1998]. The natural variability in surface C_T that ranges up to 15% of the mean value varies with location and season. In contrast, the annual anthropogenic CO_2 uptake in the upper ocean is 1 or 2 orders of magnitude smaller than the natural variability. The oceanic response to the anthropogenic CO_2 increase in the atmosphere can be better predicted if natural variability can be parameterized with commonly measured parameters [*Goyet and Davis*, 1997].

The first major attempts to relate surface C_T with other properties were made using the Geochemical Ocean Section Study (GEOSECS) and Transient Tracers in the Ocean/North Atlantic Study (TTO/NAS) data set [*Takahashi et al.*, 1980; *Brewer et al.*, 1995]. These studies were limited by uncertainties in accuracy and precision of C_T measurements and by spatially insufficient data coverage. Over the last 10 years, significant improvements have been made in the measurement of C_T in seawater [*Johnson et al.*, 1987, 1993]. Multinational and multiagency efforts to execute a global survey of the oceanic carbonate system during the 1990s have created a comprehensive global database of C_T. The measurement campaigns include parts of the Joint Global Ocean Flux Study (JGOFS), the National Oceanic and Atmospheric Administration/Ocean Atmosphere Carbon Exchange Study (NOAA/OACES), and the Department of Energy/World Ocean Circulation Experiment (DOE/WOCE) CO_2 survey programs.

Surface C_T algorithms are useful for studying several aspects of the marine carbonate system. Empirical surface C_T algorithms aid in estimating regional and global inventories of anthropogenic CO_2 [*Chen et al.*, 1982]. In this case, the relationships are used to correct the measured C_T for changes resulting from oxidation of organic matter after it lost contact with the surface. Surface C_T algorithms can also be used to estimate biologically produced O_2 in the mixed layer and thus new production in the ocean from the rate of change of heat storage and the change of C_T with sea surface temperature (SST), expressed as C_T/SST relationships [*Keeling et al.*, 1993]. No empirical algorithms of C_T with SST or C_T with SST and NO_3^- are presently available for much of the ocean.

This paper uses measurements from all of the OACES and some of the WOCE cruises to determine relationships between salinity (S)-normalized C_T ($NC_T = C_T \times 35/S$), SST, and NO_3^-. The OACES data sets are mainly from meridional sections, while the WOCE data sets are from zonal sections. For comparison and seasonal extrapolation the monthly mean global

[1]Rosenstiel School of Marine and Atmospheric Science/CIMAS, University of Miami, Florida.
[2]Atlantic Oceanographic and Meteorological Laboratory, NOAA, Miami, Florida.
[3]Pacific Marine Environmental Laboratory, NOAA, Seattle, Washington.
[4]Rosenstiel School of Marine and Atmospheric Science/MAC, University of Miami, Miami, Florida.

Paper number 1998GB001087.
0886-6236/00/1998GB001087$12.00

surface partial pressure of CO_2 (pCO_{2sw}) fields of *Takahashi et al.* [1997] are combined with surface alkalinity (A_T) fields of *Millero et al.* [1998] to construct the C_T fields. The surface pCO_{2sw} fields are on a 4° latitude × 5° longitude grid for a composite non-El Niño year (1990) using measurements made over the last 30 years. The surface A_T fields are produced from regional relationships of salinity-normalized A_T ($NA_T = A_T \times 35/S$) with SST using measurements made from 1991 to 1996 and data from the GEOSECS and TTO studies.

2. Methods and Data Analysis

2.1. Determination of Total Inorganic Carbon

The C_T of seawater is defined as $C_T = [CO_2^*] + [HCO_3^-] + [CO_3^{2-}]$, where brackets represent total concentrations of these constituents in seawater (μmol kg^{-1}) and $[CO_2^*]$ represents the sum of H_2CO_3 and gaseous CO_2. Recent C_T measurements have been made coulometrically using single-operator multiparameter metabolic analyzers (SOMMA) [*Johnson et al.*, 1987, 1993]. The data from these cruises are accurate to about ±2 μmol kg^{-1} (1σ), which is based on measurements of certified reference materials (CRMs) used on all the cruises (A.G. Dickson, Reference material batch information, available on the World Wide Web at http://www.mpl.ucsd.edu/people/adickson/CO2_QC/Level1/Batches.html) [*Lee et al.*, 1997; *Feely et al.*, 1999a] (see also R.M. Key, WOCE Indian Ocean Survey: Data comparison at crossover stations, available on the World Wide Web at http://geoweb.princeton.edu/staff/Key/key.cross/crossover.html). In the Atlantic Ocean we also use data from the TTO/NAS [*PCODF*, 1986a], the TTO/Tropical Atlantic Study (TTO/TAS) [*PCODF*, 1986b], and the South Atlantic Ventilation Experiment (SAVE) [*ODF*, 1992a,b]. The C_T data during the TTO/NAS and TTO/TAS cruises were obtained using potentiometric titration with an estimated precision and accuracy of ±5 μmol kg^{-1} [*Brewer et al.*, 1986]. During the SAVE cruise, C_T measurements were made coulometrically with a precision of ±2 μmol kg^{-1}, but no CRMs were available (T. Takahashi, personal communication). A summary of the field measurements used in this study is given in Table 1, and the locations of sampling stations are shown in Plate 1. The data used are available at the Carbon Dioxide Information Analysis Center (http://cdiac.esd.ornl.gov) and the NOAA/OACES site (http://www.aoml.noaa.gov/ocd/oaces). The data sets given in Table 2 and shown as green pluses in Plate 1 are used to validate the derived NC_T algorithms.

2.2. Consistency of C_T Values

The C_T data obtained from different cruises must be checked to ensure mutual consistency of the data before the algorithms are derived. All recent cruise data except for TTO and SAVE data are normalized using the CRMs analyzed during the cruises prior to the intercomparisons. The magnitude of these adjustments for all the cruise data is <3 μmol kg^{-1}. Furthermore, the data sets are compared for deep water in regions where cruise

Table 1. Summary of Cruise Data Used to Generate the Fits Shown in Tables 3 to 5

Ocean	Cruise	Year (month)	Description	Stations
Atlantic	OACES	1991 (July)	along 25°W (5°N-43°S)	33
Atlantic	OACES	1993 (July-Aug.)	along 20°W (5°S-63°N)	60
Atlantic	OACES	1998 (Jan.-Feb.)	along 24°N (75°W-15°E)	83
Atlantic	A12/A21	1990 (Jan.-Mar.)	35°S-65°S, 0°-60°W	110
Atlantic	A1E	1991 (Sept.)	50°N-60°N, 20°W-50°W	40
Atlantic	TTO/NAS	1981 (Apr.-Oct.)	North Atlantic	250
Atlantic	TTO/TAS	1982-1983 (Dec.-Feb.)	tropical Atlantic	132
Atlantic	SAVE	1987-1989 (Nov.-Apr.)	South Atlantic	370
Pacific	CGC91	1991	along 170°W (20°N-60°N)	40
Pacific	EQPAC spring	1992	equatorial Pacific	95
Pacific	EQPAC fall	1992	equatorial Pacific	107
Pacific	P15S	1996 (Feb.-Mar.)	along 170°W (67°S-equator)	144
Pacific	P18	1994 (Feb.-Apr.)	along 103°W (67°N-23°N)	184
Pacific	P14N	1993 (July-Aug.)	along 180°W (16°S-60°N)	92
Pacific	P14S	1996 (Jan.-Feb.)	along 170°E (43°S-65°S)	33
Pacific	P21	1994 (Apr.-June)	along 17°S (70°W-170°E)	194
Pacific	P16	1991 (Aug.-Oct.)	along 150°W (20°N-40°S)	130
Pacific	P17	1991 (July-Aug.)	along 135°W (5°S-35°S)	54
Pacific	S4(P)	1994 (Feb.-Apr.)	along 67°S (170°E-70°W)	112
Indian	I8 repeat (OACES)	1995 (Oct.-Nov.)	along 80°E (43°S-10°S)	108
Indian	I3	1995 (Apr.-June)	along 20°S (50°E-115°E)	130
Indian	I8 (WOCE)	1995 (Mar.-Apr.)	along 80°E (34°S-5°S)	100
Indian	I1W	1995 (Aug.-Oct.)	along 15°S (50°E-80°E)	90
Indian	S4(I)	1996 (May-July)	along 65°S (20°E-110°E)	154

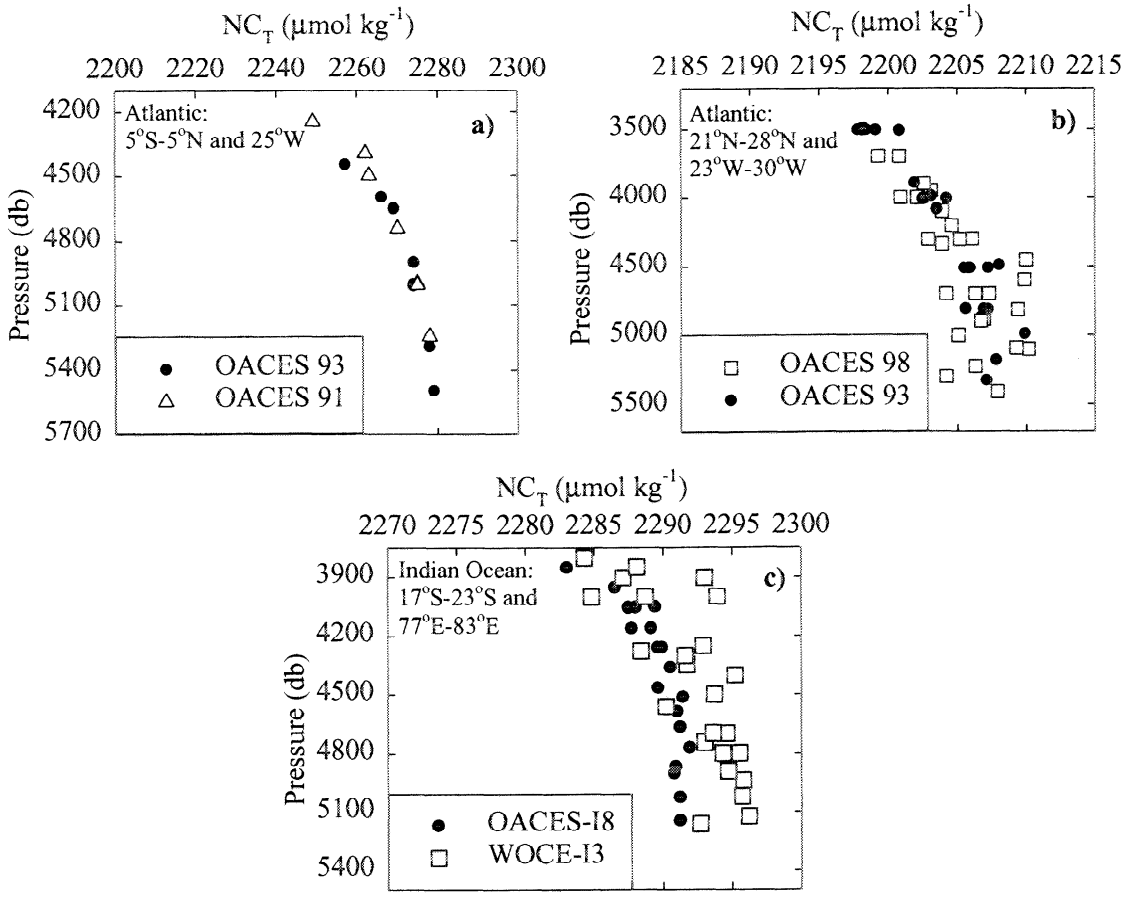

Figure 1. (a and b) NC_T versus depth in the region below 4000 m from 5°N to 5°S along 25°W and in the region below 3500 m from 21° to 28°N and 23° to 30°W in the Atlantic Ocean. (c) The NC_T versus depth in the region from 17° to 23°S and 77° to 83°E in the Indian Ocean.

tracks cross (so-called crossover analyses), assuming that the C_T in deep water does not change on subdecadal timescales.

In the Atlantic Ocean, comparisons of NC_T at the OACES 91 and OACES 93 stations between 5°N and 5°S are shown in Figure 1a. The NC_T data for depths below 3500 m for these stations agree to within ±3 μmol kg^{-1}. The measurements of NC_T made during the OACES 93 cruise are also compared with those of the OACES 98 cruise in the region from 21°N to 28°N

Table 2. Summary of Cruise Data Used to Validate the Fits Shown in Tables 3 to 5

Ocean	Cruise	Year (month)	Description	Stations	ΔC_T[a]
Atlantic	A22	1997 (Aug.-Sept.)	along 66°W (10°N-40°N)	77	-6 ± 10
Pacific	P6	1992 (May-July)	along 32°S (70°W-170°E)	267	1 ± 13
Pacific	P10	1993 (Oct.-Nov.)	along 145°E (4°S-35°N)	94	1 ± 6
Pacific	P16AP17A	1992 (Oct.-Nov.)	along 150°W (40°S-65°S) along 135°W (22°S-56°S)	127	-3 ± 8
Pacific	P19	1993 (Feb.-Apr.)	along 85°W (15°N-53°S)	188	15 ± 12
Indian	I2	1995 (Dec.)	along 10°S (45°E-105°E)	166	4 ± 8
Indian	I7N	1995 (July-Aug.)	along 60°E (20°S-25°N)	148	1 ± 8
Indian	I9N	1995 (Jan.-Mar.)	along 95°E (30°S-20°N)	129	7 ± 8
Indian	I8SI9S	1995 (Jan.)	along 95°E and 110°E (30°S-65°S)	143	2 ± 11

These data were not used to generate the fits.

[a]ΔC_T (μmol kg^{-1}) represents the mean of individual differences between the measured C_T and C_T estimated using the derived NC_T algorithms.

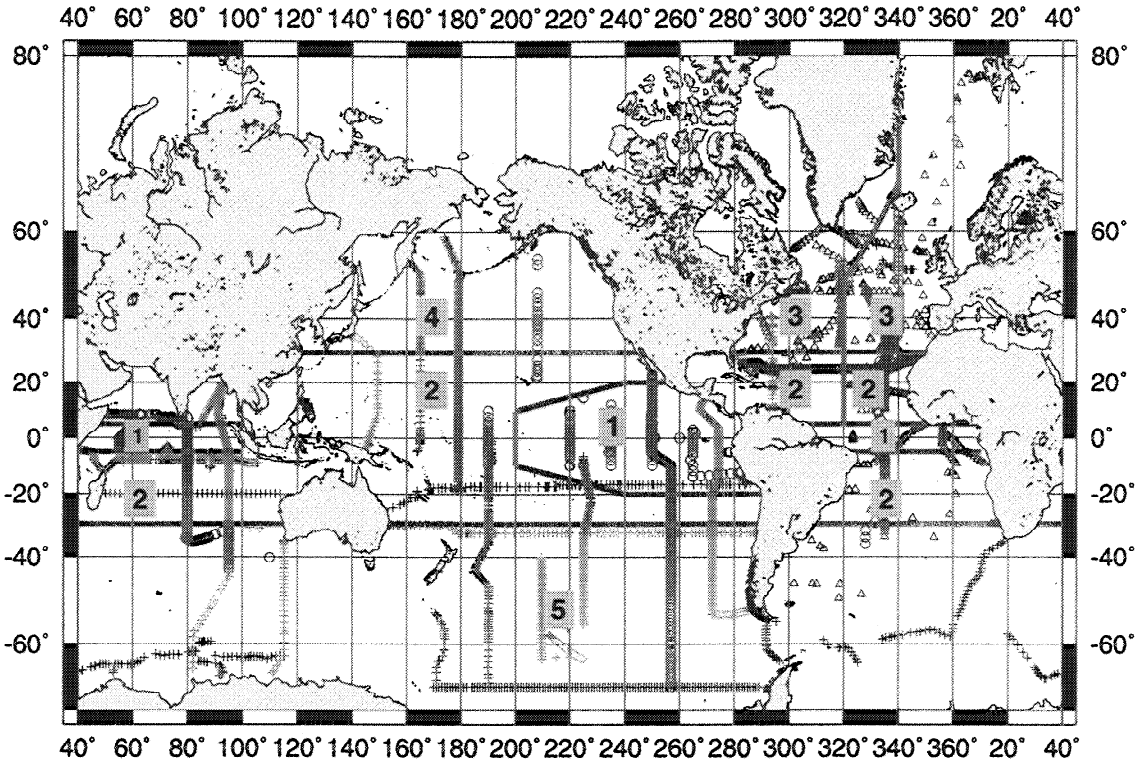

Plate 1. Location of surface data used in this analysis. They include all of the Ocean Atmosphere Carbon Exchange Study (OACES) (1991-1998) (blue circles), Transient Traces in the Ocean (TTO) (1981-1983) (blue triangles), and South Atlantic Ventilation Experiment (SAVE) (1987-1989) cruises (blue triangles) and some of the World Ocean Circulation Experiment (WOCE) (1990-1996) (blue pluses) cruises. Cruise data shown in green pluses are used to estimate uncertainties in estimating C_T using the derived salinity ($S = 35$) normalized C_T (NC_T) algorithms in Tables 3-5. Red lines represent the dynamic boundaries for the five different regions with unique relationships.

and from 23°W to 30°W at depths below 3500 m. The NC_T values obtained from these cruises are within ±2 μmol kg^{-1} (Figure 1b). In the Pacific Ocean, carbon data from cruises conducted in 1990-1996 are compared at 30 locations where cruise tracks cross [*Feely et al.*, 1999a]. The agreement for deep water with $\sigma_\theta \geq 27.0$ is within ±3 μmol kg^{-1}. Similar comparisons have been made for the WOCE carbon measurements in the Indian Ocean (R.M. Key; see http://geoweb.princeton.edu/staff/Key/key.cross/crossover.html). In addition, crossover NC_T data for depths below 3500 m from OACES I8 repeat and WOCE I3 agree to within ±3 μmol kg^{-1} (Figure 1c).

To account for surface water C_T increases due to rising atmospheric CO_2 concentration, all the C_T data are normalized to the year 1990, which is chosen to match with the global climatology of pCO_{2SW} [*Takahashi et al.*, 1997]. In (sub)tropical regions, vertical mixing of surface waters with subsurface waters is limited due to strong stratification, and the mean surface C_T concentration increases with a rate similar to the atmospheric CO_2 increase. This has been shown for C_T and pCO_{2SW} trends in the Sargasso Sea [*Takahashi et al.*, 1983; *Bates et al.*, 1996], at the Hawaii Ocean Time-series site [*Winn et al.*, 1998], in the central equatorial Pacific [*Feely et al.*, 1999b], and in the western North Pacific between 3°N and 35°N [*Inoue et al.*, 1995]. An adjustment of 1 μmol kg^{-1} per year is applied to C_T measurements made on the (sub)tropical waters between 30°N and 30°S. The accuracy of adjusted C_T data from TTO and SAVE studies is assessed by comparing them with the

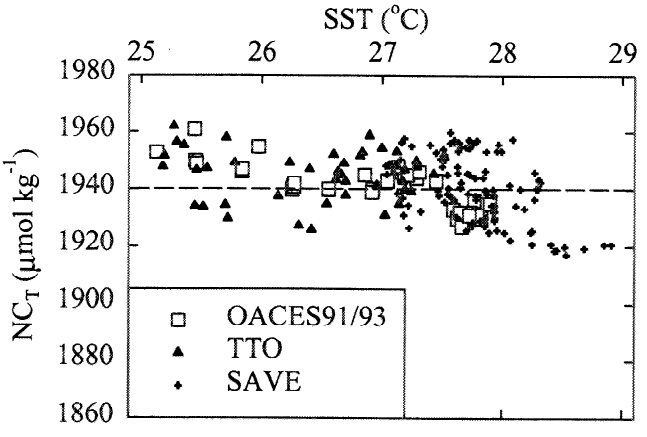

Figure 2. Comparison of OACES 91/93 surface NC_T at SST >25°C with older data from TTO/NAS and SAVE studies. The dashed line represents the mean of all the data.

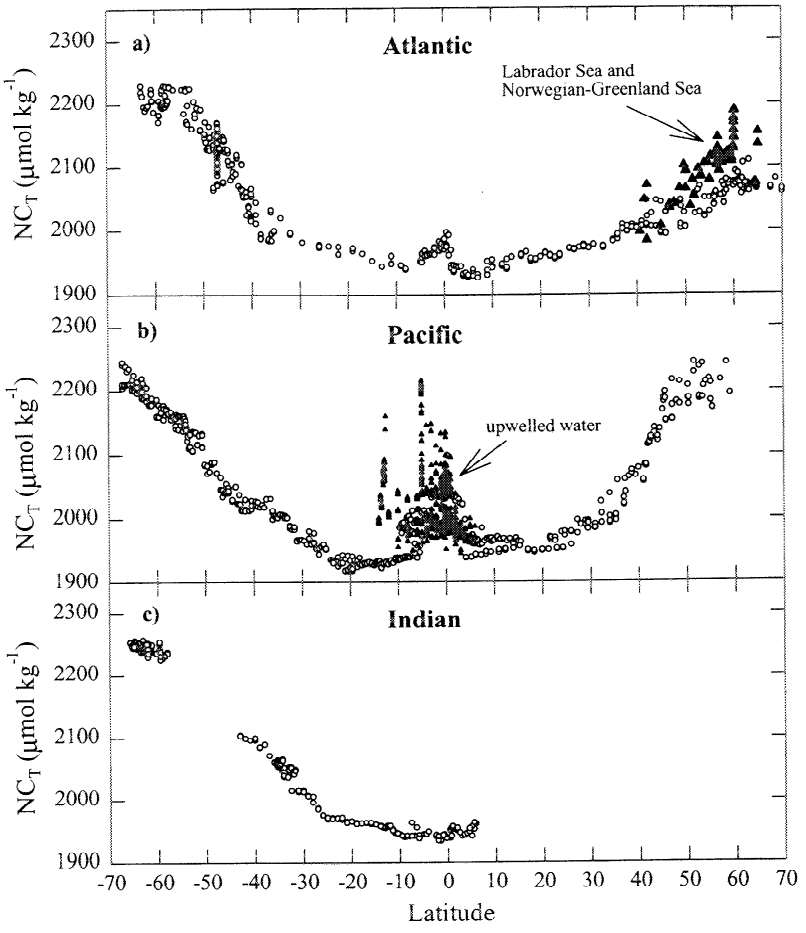

Figure 3. Distribution of NC_T as a function of latitude in the (a) Atlantic, (b) Pacific, and (c) Indian Oceans. The NC_T data obtained from the Norwegian-Greenland Sea and from zone 1 in Plate 1 are shown in filled triangles in (a) and (b), respectively.

recent cruise data in the Atlantic. The OACES 91/93 NC_T data (NC_T = 1942 ± 8 μmol kg^{-1}, n=37) at temperatures >25°C are in good agreement with TTO/TAS (NC_T = 1945 ± 9 μmol kg^{-1}, n=65) and SAVE (NC_T = 1940 ± 12 μmol kg^{-1}, n=134) data (Figure 2). No correction is applied to C_T measurements made on high-latitude waters (>30°) since outcropping of deep isopycnal surfaces dilutes the small signals of anthropogenic CO_2 component throughout the entire water column. For instance, the temperature-normalized surface pCO_{2SW} measurements made by *Wong and Chan* [1991] in 1974-1979 at Ocean Station P (50°N, 145°W) in the northeastern subarctic Pacific are nearly the same as the 1985-1989 observations by *Takahashi et al.* [1993] and the 1986 observations by *Murphy et al.* [1995]. We cannot rule out the possibility that surface pCO_{2SW} might increase in other subpolar and polar regions where vertical exchange of water is weaker and the duration of exposure time is longer, albeit at a slower rate than in the (sub)tropics [*Takahashi et al.*, 1997]. Although measurements are needed to quantify the C_T increase in high-latitude waters due to oceanic uptake of anthropogenic CO_2, the corrections are relatively small as most data used in this study were obtained within 5 years of 1990.

3. Parameterization of Surface Total Inorganic Carbon

3.1. General Trends of C_T in Surface Oceans

The surface C_T concentration is influenced by lateral and vertical mixing of water with different levels of C_T (the

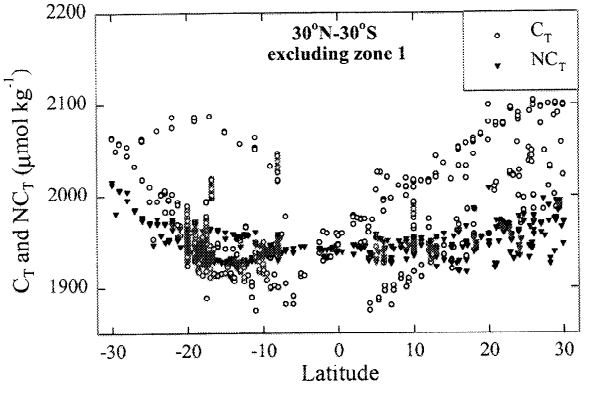

Figure 4. Comparison of C_T with NC_T for waters in areas between 30°N and 30°S excluding the upwelling regions.

Table 3. Regional Representations of Salinity (S=35) Normalized C_T (NC_T) for Equatorial Upwelling Regions for 1990

Region	Equation[a]	SST, °C	Regional NC_T Equations	σ[b]	N[c]
			NO_3^- > 0.5 μmol kg^{-1}		
			equatorial regions other than the north equatorial Pacific		
Zone 1	1	18°-29°C	NC_T = 1940 − 10.327 (SST−29) − 0.451 (SST−29)^2 + 7.829 NO_3^-	±8.1	550
			north equatorial Pacific		
Zone 1	2	18°-29°C	NC_T = 1950 − 7.604 (SST−29) − 0.178 (SST−29)^2 + 6.883 NO_3^-	±7.0	550
			NO_3^- < 0.5 μmol kg^{-1}		
			equatorial regions other than the north equatorial Pacific		
Zone 1	3	20°-29°C	NC_T = 1940 − 11.976 (SST−29) − 0.513 (SST−29)^2	±6.2	124
			NC_T = 1940 at SST > 29°C	±6.5	60
			north equatorial Pacific		
Zone 1	4	20°-29°C	NC_T = 1950 − 5.549 (SST−29) + 0.125 (SST−29)^2	±6.3	124
			NC_T = 1950 at SST > 29°C	±7.0	45
			Bay of Bengal: NO_3^- < 0.5 μmol kg^{-1}		
Zone 1	5	20°-29°C	NC_T = 1940 − 33.385 (SST−29) − 2.407 (SST−29)^2	±7.5	72
			NC_T = 1940 at SST > 29°C	±6.5	40

Zone 1 is the equatorial Pacific within 75°W-110°W, 20°N-20°S and 110°W-160°W, 10°N-10°S, Atlantic between 5°N and 5°S, and the Indian between 5°N and 5°S.

[a]Austral summer (S) is from October-April and austral winter (W) is from May-September, while boreal summer/winter is opposite. Equations without S or W can be used for the entire year.

[b]Root mean square deviation $\sigma = \{\Sigma(\Delta)^2/(N-1)\}^{0.5}$, where Δ is the difference between the measured values and those calculated from the equation.

[c]N is the number of data points used for fit.

transport effect), photosynthesis and oxidation of organic matter (the biological effect), and changes in temperature and salinity [*Poisson et al.*, 1993; *Takahashi et al.*, 1993]. These effects are directly or indirectly correlated with SST, but trends often differ seasonally and geographically. Since the boundaries of the derived NC_T algorithms described below are primarily derived as a function of SST, the geographic boundary for a particular algorithm is dynamic and will vary depending on the seasonal SST for the particular region.

Several general trends in NC_T are found in the world oceans. Except for the equatorial upwelling regions where the NC_T sharply increases near the equator, the NC_T shows weak trends with SST in areas between 30°N and 30°S (Figure 3). In these regions, ~70% of the spatial and seasonal surface C_T variations of up to 250 μmol kg^{-1} can be removed by normalizing the results to a constant salinity (S=35) [*Bates et al.*, 1996; *Winn et al.*, 1998] (Figure 4). In the equatorial upwelling areas the distribution of surface NC_T is, to a large extent, controlled by the upwelling rate of subsurface water with high NC_T; thus, changes in NC_T are inversely correlated with SST. Since a part of the change in NC_T is attributed to biological activity, the values of NC_T obtained on the upwelled waters are parameterized with a physical (SST) and a biological parameter (nitrate).

At latitudes (>30°) where SST is <20°C, the NC_T increases during the seasonal cooling due to the convective mixing of deep waters rich in NC_T. In this case, NC_T increases by seasonal cooling are inversely correlated with SST. In springtime, the shallow mixed layer formation and surface warming facilitate phytoplankton blooms, which cause rapid decrease in surface C_T. These changes occur in tandem with SST increase and are directly reflected in decreasing nitrate concentration (NO_3^-). Thus surface NC_T values in high-latitude waters are related with SST and NO_3^-. Parameterizations of NC_T with SST and NO_3^- are expanded below for different regions of the oceans.

3.2. Equatorial Upwelling Regions (Zone 1)

The oceanic equatorial regions shown in Plate 1 are the largest oceanic source of CO_2 to the atmosphere due to upwelling of CO_2-rich subsurface waters [*Keeling*, 1968; *Andrié et al.*, 1986; *Tans et al.*, 1990; *Inoue et al.*, 1995; *Feely et al.*, 1987, 1995, 1997, 1999b; *Takahashi et al.*, 1997]. Particularly, the NC_T concentration in the central and eastern equatorial Pacific is governed by the upwelling intensity and source of upwelled waters which is influenced by the El Niño/Southern Oscillation cycle [*Winguth et al.*, 1994; *Feely et al.*, 1995, 1997]. The elevated NC_T in the upwelled waters is attenuated by biological processes, loss of CO_2 to the atmosphere, and mixing with surrounding waters with lower NC_T, while the water is transported from the site of upwelling by advection [*Murray et al.*, 1994].

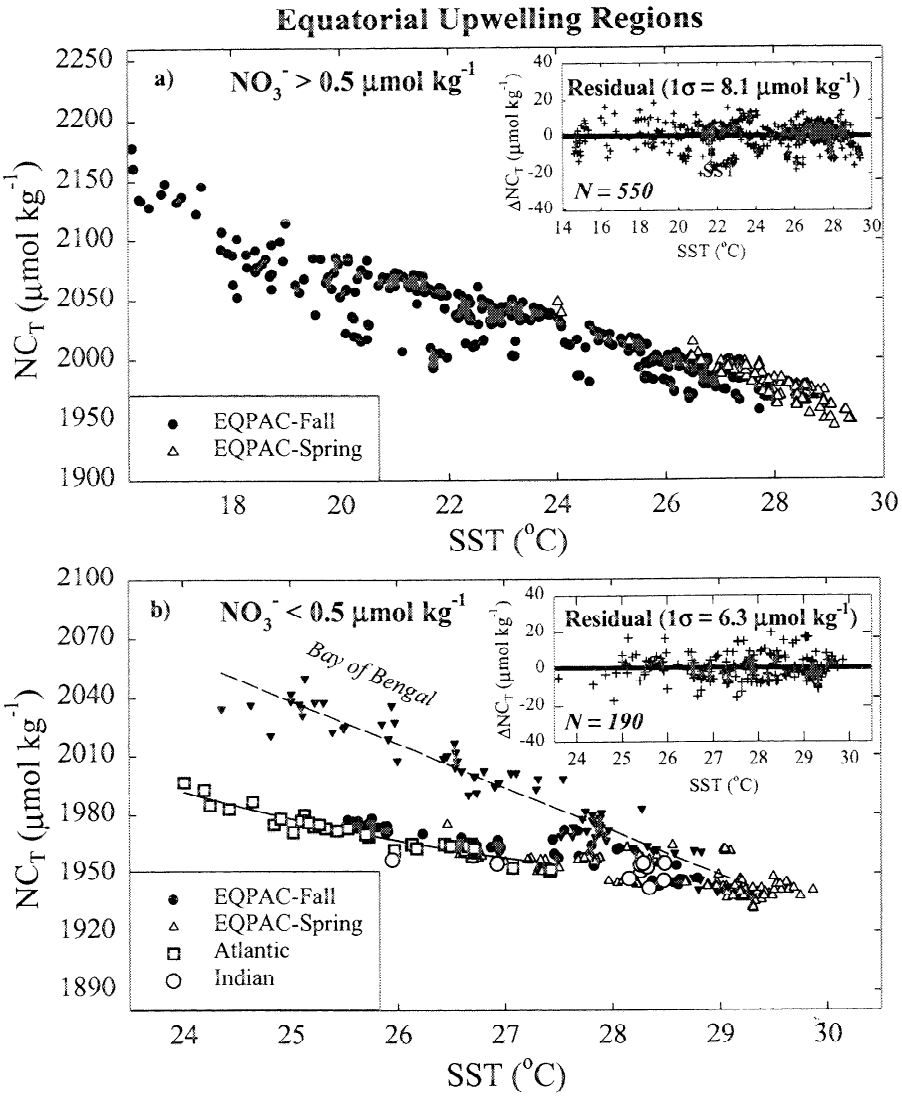

Figure 5. Plots of NC_T versus SST in the upwelled waters in the eastern equatorial Pacific (75°-120°W and 20°N-20°S, 120°-160°W and 10°N-10°S), in the Atlantic (5°N-5°S), and in the Indian Ocean (5°N-5°S). The NC_T values for waters with (a) higher and (b) lower than 0.5 µmol kg^{-1} of NO_3^- are plotted as a function of SST. The NC_T trend found for the Bay of Bengal is shown in Figure 5b (solid triangles). Inserts are residual plots of ΔNC_T (ΔNC_T = measured NC_T - calculated NC_T from the derived NC_T algorithms).

Measurements made during the NOAA/NSF sponsored U.S. JGOFS Equatorial Pacific Process Study in the boreal spring and fall of 1992 are used to generate the fit for this region. The spring data are taken during El Niño conditions, and the fall data are taken during non-El Niño conditions. The SST of 26°-30°C observed during the spring are 1°-2°C higher than the climatological values for the corresponding months, while the SST of 18°-28°C during the fall are only 0.1°-1°C higher than the fall mean SST at the eastern equatorial Pacific.

The NC_T data with NO_3^- >0.5 µmol kg^{-1} are fit to functions of SST and NO_3^- to account for the effects of upwelled water and biology on the NC_T trend for this region (equations (1) and (2) in Table 3; see Figure 5a). Waters with NO_3^- <0.5 µmol kg^{-1} in zone 1 have considerably higher values of NC_T than in other waters in the latitude band of 30°N-30°S (zone 2). To obtain a smooth transition between the equatorial upwelling regions (zone 1) and the (sub)tropical regions (zone 2), the NC_T values with NO_3^- <0.5 µmol kg^{-1} in the equatorial upwelling regions are fit to a second-order polynomial in SST and forced to intersect the algorithms for the other regions (equations (3) and (4) in Table 3; see Figure 5b).

Waters with temperatures >29°C have a constant NC_T value of 1950 ± 7 µmol kg^{-1} for the north equatorial Pacific (75°-110°W and 20°N-0°; 110°-160°W and 10°N-0°) and of 1940 ± 6 µmol kg^{-1} for the other equatorial regions. Although the upwelling is less intense in the equatorial Atlantic (5°S-5°N) and Indian (5°S-5°N) Oceans, elevated values of NC_T are often found while NO_3^- concentration is at or below the detection limit. Equation (3) is valid for these regions as well. A separate equation is derived for the Bay of Bengal (Table 3) because the

Table 4. Regional Representations of Salinity (S=35) Normalized C_T (NC_T) for Areas Between 30°N and 30°S Excluding Zone 1 for 1990

Region	Equation[a]	SST, °C	Regional NC_T Equations	σ[b]	N[c]
			(sub)tropics other than the western (sub)tropical Atlantic and north (sub)tropical Pacific		
Zone 2	6S	20°-29°C	$NC_T = 1940 - 3.039\,(SST-29) + 0.494\,(SST-29)^2$	±7.5	320
Zone 2	6W	20°-29°C	$NC_T = 1940 - 1.003\,(SST-29) + 0.372\,(SST-29)^2$	±4.9	110
			$NC_T = 1940$ at SST > 29°C	±6.7	275
			north (sub)tropical Pacific		
Zone 2	7S	20°-29°C	$NC_T = 1950 + 0.188\,(SST-29) + 0.725\,(SST-29)^2$	±8.0	320
Zone 2	7W	20°-29°C	$NC_T = 1950 + 2.570\,(SST-29) + 0.640\,(SST-29)^2$	±5.2	110
			$NC_T = 1950$ at SST > 29°C	±8.0	165
			western (sub)tropical Atlantic (west of 40°W); summer and winter		
Zone 2	8	20°-29°C	$NC_T = 1940 + 1.842\,(SST-29) + 0.468\,(SST-29)^2$	±6.2	230
			$NC_T = 1940$ at SST > 29°C	±6.1	25

Zone 2 is the area between 30°N and 30°S excluding zone 1.
[a]See Table 3 for definition.
[b]See Table 3 for definition.
[c]See Table 3 for definition.

values of NC_T are ~30-80 μmol kg^{-1} greater than observations at the same SST from other upwelling regions where NO_3^- concentration is <0.5 μmol kg^{-1}. The higher values of NC_T for waters in the Bay of Bengal can be attributed to freshwater influx with high NC_T from rivers.

3.3. Regions between 30°N and 30°S Excluding Equatorial Upwelling (Zone 2)

The observed NC_T variations in the (sub)tropics weakly correspond to changes in SST. The maximum difference in the summer-winter values of NC_T is found in areas near 30°N or 30°S, where SST is between 17° and 25°C. For a given SST, summer surface values of NC_T are ~20-30 μmol kg^{-1} higher than the wintertime values. Thus the summer and winter surface results (20° < SST < 29°C) are separately fit to a second-order polynomial in SST and forced to an intercept of 1950 for the North Pacific and an intercept of 1940 for the Atlantic, Indian, and South Pacific Oceans. This yields a smooth transition of NC_T in the warmer waters (equations (6) and (7) in Table 4) (Figure 6). Waters with SST >29°C have a constant value of $NC_T = 1950 \pm 8$ μmol kg^{-1} for the northern (sub)tropical Pacific and of $NC_T = 1940 \pm 7$ μmol kg^{-1} for the other (sub)tropical regions.

A single annual NC_T/SST relationship representing the western (sub)tropical Atlantic (west of 40°W) is derived using winter (Bermuda Atlantic Time-series Study (BATS), OACES 98) and summer (BATS, TTO) surface NC_T data (equation (8) in Table 4) since the winter-summer NC_T differences are statistically insignificant (Figure 6c). Mixing along shallow isopycnal surfaces yields small changes in NC_T, which causes a weaker NC_T/SST relationship than the derived values for similar geographic regions of the eastern Atlantic, Pacific, and Indian Oceans. Monthly mean NC_T data from 1988 to 1993 at the BATS site are also in good agreement with the estimated values using equation (8) in Table 4. We cannot rule out the possibility that the east-west difference in NC_T algorithms might exist in other basins, but there are no data to confirm this possibility.

Equations (6)-(8) in Table 4 are valid only for SST between 20° and 29°C and apply to geographic regions approximately between 30°N and 30°S. For waters with SST <20°C typically found in these regions during winter, the relationships (9)-(12) in Table 5 should be used to predict NC_T.

3.4. Regions North of 30°N (Zones 3 and 4)

For SST <20°C corresponding to latitudes between 30° and 70°N, NC_T increases with latitude and NO_3^-. Seasonally different coefficients are derived for equations of the same functional form for the western North Atlantic, eastern North Atlantic, and North Pacific Oceans (Figure 7, Table 5). Each equation has an intercept of 1980 μmol kg^{-1} for boreal winter and 2010 μmol kg^{-1} for boreal summer. Different intercepts are needed at SST=20°C to fit the summer and winter values of NC_T for continuity between these areas and the (sub)tropics (zone 2). For a given SST, the North Pacific and Southern Ocean surface waters contain values of NC_T 60-100 μmol kg^{-1} greater than those of the eastern North Atlantic. This is attributed to the outcropping of deep waters with higher NC_T in the North Pacific and Southern Ocean.

Equations (6)-(8) in Table 4 should be used for waters with SST >20°C generally found in areas between 30° and 40°N during summer since equations (9)-(11) in Table 5 are valid for SST <20°C.

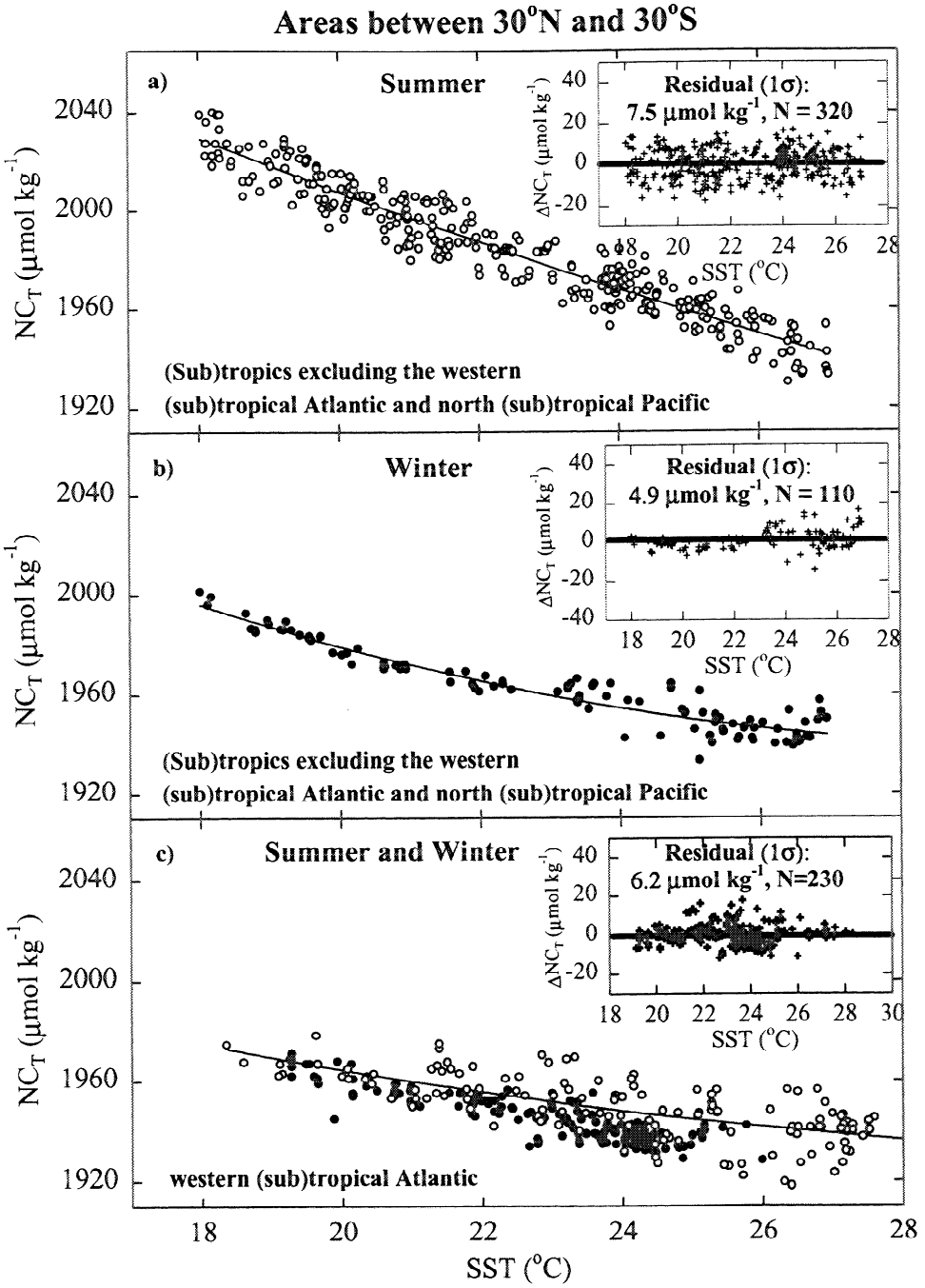

Figure 6. Plots of (a) summer and (b) winter NC_T versus SST in areas between 30°N and 30°S excluding the upwelling regions (zone 1) and the western (sub)tropical Atlantic. (c) Summer and winter surface NC_T data in the western (sub)tropical Atlantic fit to the same equation. The solid lines are the results of regressions. Inserts are residual plots of ΔNC_T (ΔNC_T = measured NC_T − calculated NC_T from the derived NC_T algorithms).

Table 5. Regional Representations of Salinity (S=35) Normalized C_T (NC_T) for Regions at Latitudes Higher than 30° for 1990

Region	Equation[a]	SST, °C	Regional $NTCO_2$ Equations	σ[b]	N[c]
			western North Atlantic (west of 40°W)		
Zone 3	9S	<20°C	$NC_T = 2010 - 8.633\,(SST-20) - 0.036\,(SST-20)^2 - 0.279\,NO_3^-$	±6.9	40
			$[2010 - 8.500\,(SST-20) - 0.031\,(SST-20)^2]$[d]	[±8.5]	40
Zone 3	9W	<20°C	$NC_T = 1980 - 14.680\,(SST-20) - 0.297\,(SST-20)^2 - 1.153\,NO_3^-$	±7.5	40
			$[2010 - 14.131\,(SST-20) - 0.272\,(SST-20)^2]$	[±10.8]	40
			eastern North Atlantic (east of 40°W)		
Zone 3	10S	<20°C	$NC_T = 2010 - 4.262\,(SST-20) - 0.013\,(SST-20)^2 + 5.054\,NO_3^-$	±5.9	124
			$[2010 - 8.646\,(SST-20) - 0.249\,(SST-20)^2]$	[±9.3]	124
Zone 3	10W	<20°C	$NC_T = 1980 - 10.864\,(SST-20) - 0.311\,(SST-20)^2 + 4.235\,NO_3^-$	±6.7	124
			$[1980 - 14.538\,(SST-20) - 0.510\,(SST-20)^2]$	[±13]	124
			North Pacific		
Zone 4	11S	<20°C	$NC_T = 2010 - 7.805\,(SST-20) + 0.069\,(SST-20)^2 + 3.891\,NO_3^-$	±7.8	73
			$[2010 - 6.926\,(SST-20) + 0.453\,(SST-20)^2]$	[±18]	73
Zone 4	11W	<20°C	$NC_T = 1980 - 13.199\,(SST-20) - 0.172\,(SST-20)^2 + 3.983\,NO_3^-$	±6.7	73
			$[1980 - 12.300\,(SST-20) + 0.222\,(SST-20)^2]$	[±16]	73
			Southern Ocean		
Zone 5	12S	<20°C	$NC_T = 2010 - 7.415\,(SST-20) + 0.024\,(SST-20)^2 + 2.343\,NO_3^-$	±6.2	685
			$[2010 - 10.144\,(SST-20) + 0.035\,(SST-20)^2]$	[±8.1]	685
Zone 5	12W	<20°C	$NC_T = 1980 - 12.884\,(SST-20) - 0.112\,(SST-20)^2 + 1.365\,NO_3^-$	±6.8	685
			$[1980 - 14.473\,(SST-20) - 0.106\,(SST-20)^2]$	[±8.5]	685

Zone 3 is the North Atlantic north of 30°N, zone 4 is the North Pacific north of 30°N, and zone 5 is south of 30°S.
[a]See Table 3 for definition.
[b]See Table 3 for definition.
[c]See Table 3 for definition.
[d]This is the best fit using only SST as variable.

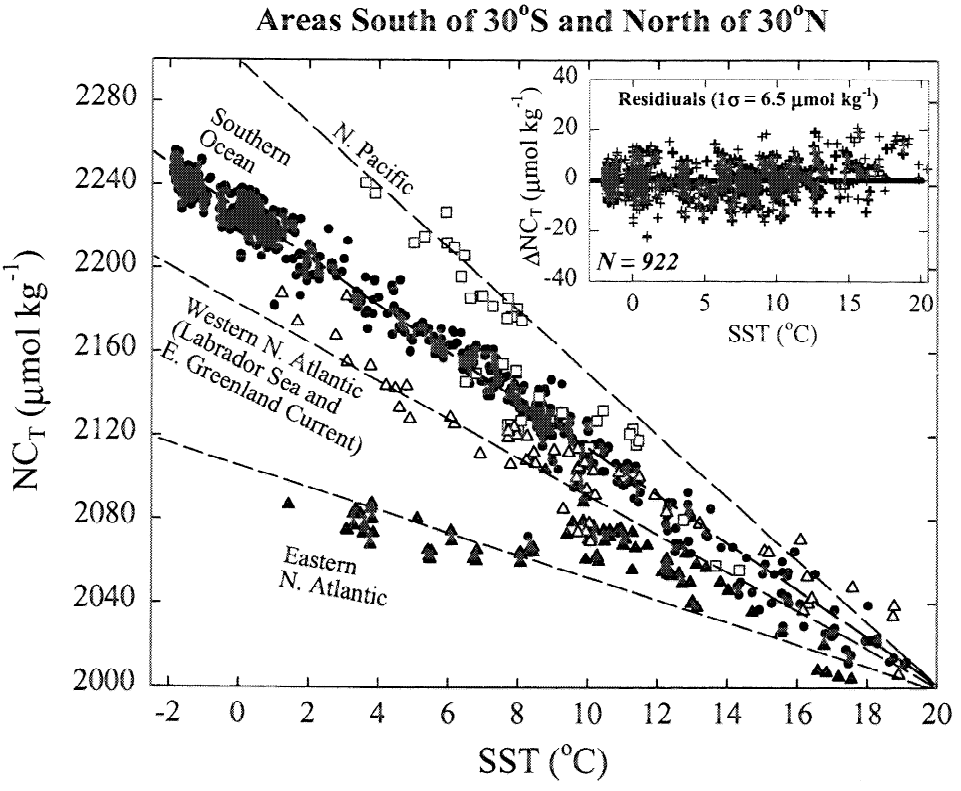

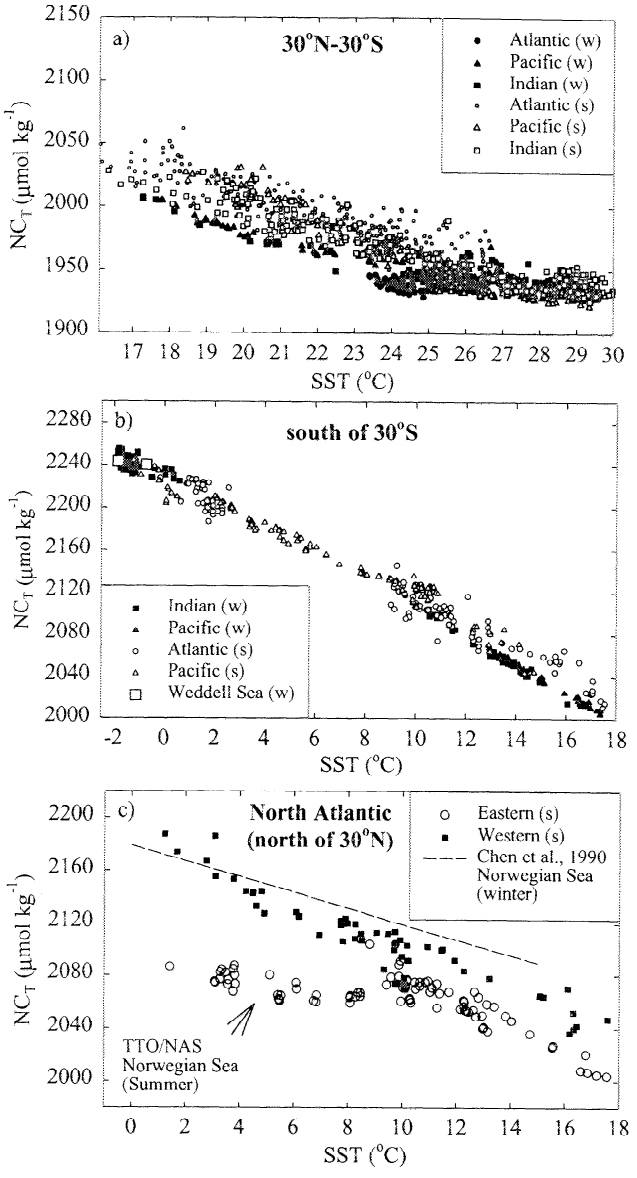

Figure 8. Winter and summer surface NC_T versus SST in areas between (a) 30°N and 30°S, (b) south of 30°S, and (c) north of 30°N. Symbols in Figures 8a and 8b are wintertime (w) (solid circles, triangles, and squares) and summertime (s) (open circles, triangles, and squares) measurements. Squares and circles in Figure 8c denote the western and eastern basins. A dashed line in Figure 8c is the relationship of *Chen et al.* [1990], which is valid between 0° and 14°C.

3.5. Regions South of 30°S (Zone 5)

Wintertime C_T data for waters south of 30°S are sparse, but good quality summertime data are available. The values of NC_T for this region are fit to functions of SST and NO_3^- with intercepts of 1980 μmol kg^{-1} for austral winter surface waters and 2010 μmol kg^{-1} for austral summer surface waters (Table 5 and Figure 7). Seasonally different intercepts are needed at SST = 20°C to fit the summer and winter values of NC_T for continuity between this region and the (sub)tropics (zone 2).

As with the northern regions, equation (12) in Table 5 is valid only at SST <20°C. Therefore equation (6) in Table 4 should be used for waters with SST >20°C in areas between 30° and 40°S during summer.

3.6. Summertime/Wintertime Differences in $NTCO_2$ Algorithms

The effect of seasonality needs to be addressed before the derived NC_T algorithms given in Tables 3-5 can be used with confidence. In the (sub)tropical oceans (zone 2 in Table 4) excluding the equatorial upwelling regions SST is typically >20°C throughout the year, and its seasonal variation ranges from 5°-6°C in latitudes near its boundaries to 2°-3°C at lower latitudes. Waters with SST >29°C corresponding to latitudes between 20°N and 20°S have a constant value of 1940 ± 7 μmol kg^{-1} regardless of season or ocean (Figure 8a). However, for SST 17°-25°C, the summer surface NC_T values are typically 20-30 μmol kg^{-1} higher than the winter values for a given SST. The greater scatters of summer surface NC_T data can be attributed to the spatial variability in biological activity.

For latitudes >30°, seasonal variations in SST range from 5°-6°C in latitudes near its boundaries to 2°-3°C in latitudes >50°. Summer and winter surface values of NC_T are compared in the Southern Ocean and North Atlantic where deep-water formation takes place in the winter. There is good agreement between winter surface values of NC_T for cruise S4I and the estimated values using the NC_T algorithm (equation (12) in Table 5) for the Southern Ocean that is constructed using mainly summer surface data (Figure 8b). An earlier study [*Poisson and Chen*, 1987] shows that the NC_T/SST relationship derived using the austral winter data from the U.S.-USSR Weddell Polynya Expedition in 1981 agrees to ±6 μmol kg^{-1} with the summer GEOSECS data (1969-1980) in the Southern Ocean. This relationship agrees to ±7 μmol kg^{-1} with the estimated values using our derived algorithm for the Southern Ocean. More recent summer and winter NC_T measurements made on Weddell Sea waters [*Hoppema et al.*, 1995, 1999] agree to ±8 μmol kg^{-1} with the calculated values using equation (12) in Table 5. In the North Atlantic we compare summer surface TTO/NAS data with winter surface data collected from the Hudson cruise (February-April 1982) in the Norwegian and Greenland Seas. For a given temperature the TTO/NAS $NTCO_2$ data are ~70 μmol kg^{-1} lower than the Hudson cruise data [*Chen et al.*, 1990] for the Norwegian and Greenland Seas (Figure 8c). This is attributed to seasonal difference in the circulation patterns. In summer the Norwegian Current, which is a continuation of the North Atlantic Current with lower NC_T, is prevalent in the Norwegian and Greenland Seas, while in winter the East Greenland Current with higher NC_T composed of the outflow of

Figure 7. Plots of NC_T versus SST in the eastern North Atlantic (30°-80°N, east of 40°W), the western North Atlantic (30°-80°N, west of 40°W), the North Pacific (30°-60°N), and the Southern Ocean (30°-70°S). The dashed lines are to aid visualization of the trends. Inserts are residual plots of ΔNC_T (ΔNC_T = measured NC_T − calculated NC_T from the derived NC_T algorithms).

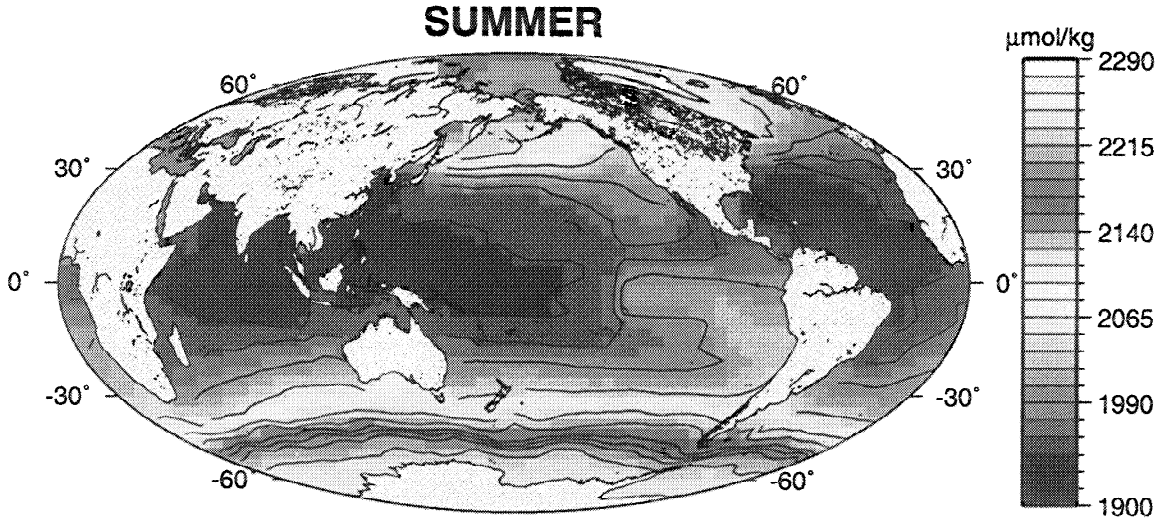

Plate 2. Summer surface values of NC_T in the major basins estimated from the derived NC_T algorithms along with the values of SST for 1990 from the National Centers for Environmental Prediction/National Center for Atmospheric Research (NCEP/NCAR) reanalysis [*Kalnay et al.*, 1996] and with annual mean NO_3^- fields from the World Ocean Atlas [*Conkright et al.*, 1994]. Annual mean NO_3^- fields are interpolated to a 4° latitude × 5° longitude grid to match with the grid size used in the pCO_{2SW} climatology.

the Arctic Sea dominates in the region. Wintertime Hudson cruise data are in good agreement with the TTO/NAS summertime data collected in the southwestward flowing East Greenland Current. When recent summer and winter measurements made on European cruises become available, the different trends of NC_T in the Nordic Sea can be further elucidated. The comparability of summer-winter data in the North Pacific cannot be examined in this paper since wintertime measurements are not publicly available in this region.

4. Global Map of C_T in the Surface Ocean

4.1. Global C_T Distribution from the Derived NC_T Algorithms

The parameterizations of NC_T with respect to SST and NO_3^- given in Tables 3-5 can be used to infer surface C_T from SST, NO_3^-, and S measurements. A global distribution of NC_T for August is constructed from the derived fits of NC_T combined with the values of SST for 1990 from the National Centers for Environmental Prediction/National Center for Atmospheric Research (NCEP/NCAR) reanalysis [*Kalnay et al.*, 1996] and with annual mean NO_3^- fields from the World Ocean Atlas 1994 [*Conkright et al.*, 1994] (Plate 2). Annual climatological NO_3^- data at high latitudes are largely composed of summertime values since most expeditions to high-latitude oceans have been made in the summer [*Conkright et al.*, 1994]. It should be possible to construct seasonal distributions of surface NC_T particularly for high-latitude regions (>30°) if the derived NC_T/SST/NO_3^- algorithms are combined with robust NO_3^-/SST relationships or if more wintertime NO_3^- data become available. Uncertainties in estimated NC_T using the derived NC_T/SST correlations (equations in brackets in Table 5) are significantly greater than using the NC_T/SST/NO_3^- correlations.

To obtain an independent error estimate, the estimated values of NC_T using the derived algorithms are compared with measurements not used to develop the same relationships. The uncertainty in estimated NC_T ranges from -3 to ±15 μmol kg^{-1} (ΔC_T in Table 2), which is somewhat greater than the area-weighed error of ±7 μmol kg^{-1}. Overall, estimated values of NC_T are in good agreement with the measured values, except for certain specific regions. The large differences off the coast of Chile (P19) are probable because the equation for the eastern equatorial Pacific (zone 1) is used in this very different oceanic regime.

4.2. Monthly Mean Global C_T Distribution from A_T and pCO_{2SW} Fields

An alternative way to estimate C_T in the upper ocean is to use the monthly climatology of pCO_{2SW} and regional algorithms of NA_T with SST and S to calculate the values of C_T. The values of pCO_{2SW} are calculated using climatological ΔpCO_2 fields [*Takahashi et al.*, 1997] and pCO_{2AIR} in the air for 1990 [*Conway et al.*, 1994]. Monthly mean global A_T fields are estimated from the regional NA_T/SST algorithms [*Millero et al.*, 1998] along with global records of SST and S obtained from the NCEP/NCAR reanalysis data set for 1990 and from the World Ocean Atlas 1994 [*Levitus et al.*, 1994], respectively. *Lee et al.* [1997] show that estimated A_T values from the derived NA_T/SST algorithms and the measured values of underway pCO_{2SW}, SST, and S yield calculated values of surface C_T that are in good agreement (±4 μmol kg^{-1}) with the coulometrically measured values for the OACES 93 North Atlantic cruise.

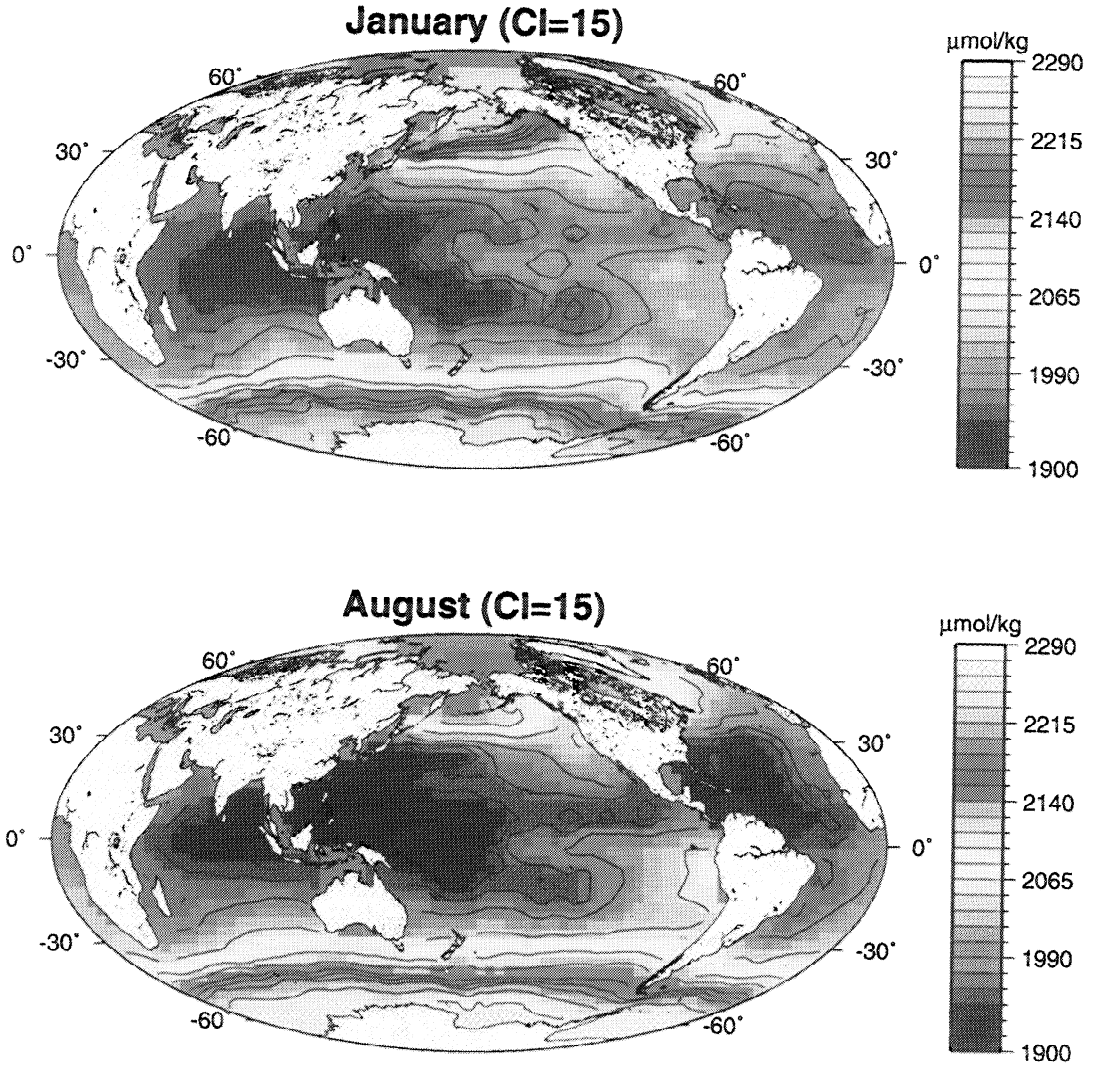

Plate 3. Mean surface values of NC_T for (a) January and (b) August of 1990 calculated from the pCO_{2sw} [*Takahashi et al.*, 1997] and A_T [*Millero et al.*, 1998] fields using the carbonic acid dissociation constants of *Mehrbach et al.* [1973] as refit by *Dickson and Millero* [1987]. The contours are at 15 µmol kg^{-1} intervals (Cl=15).

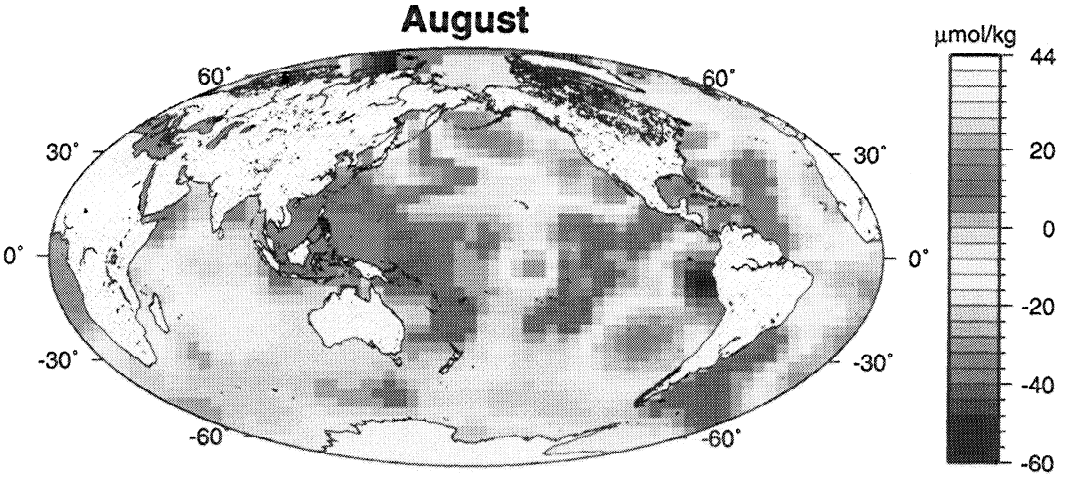

Plate 4. Differences between the values of NC_T for August estimated from the derived NC_T/SST and NC_T/SST/NO_3^- relationships with the calculated values from pCO_{2sw} [*Takahashi et al.*, 1997] and A_T [*Millero et al.*, 1998] fields.

The monthly mean global distribution of C_T on 4° × 5° pixels is constructed from A_T and pCO_{2SW} fields using the carbonic acid dissociation constants of *Mehrbach et al.* [1973] as refit by *Dickson and Millero* [1987]. The resulting C_T fields are then converted to NC_T using S fields (Plates 3a and 3b). The uncertainty associated with the calculated NC_T arises, in part, from the uncertainties in the pCO_{2SW} climatology since the monthly mean pCO_{2SW} climatology includes large oceanic areas without measurements. The accuracy of the calculated NC_T is evaluated by comparing them with field measurements. The mean difference is -4±14 μmol kg^{-1} (1σ), but larger differences are found locally (Figure 9). For instance, calculated NC_T values for waters in the eastern equatorial Pacific (10°N-10°S) are significantly smaller than the measured values in correspondence with the low climatological pCO_{2SW} values in this region.

The NC_T values for August calculated from global A_T and pCO_{2SW} fields are also compared with the estimated values using the derived NC_T algorithms and SST fields. The mean difference is -4±15 μmol kg^{-1} (1σ) (Plate 4). The differences vary regionally. The calculated NC_T values from A_T and pCO_{2SW} are slightly higher than the estimated values using the derived algorithms in the Indian and Southern Oceans but lower in the western Pacific. Possible biases in the climatological NO_3^- fields can contribute to errors in estimating C_T using the derived NC_T/SST/NO_3^- algorithms.

For validation of seasonal extrapolation the estimated NC_T values using the derived NC_T algorithms are compared with the calculated values from A_T–pCO_{2SW} fields for the western North Pacific, where pCO_{2SW} is seasonally well sampled (30°-60°N and 160°-180°E) (Figure 10). The differences are small for winter months. Systematic biases, within the range of uncertainty of -3 to ±15 μmol kg^{-1} (1σ), are found for a period from May to September.

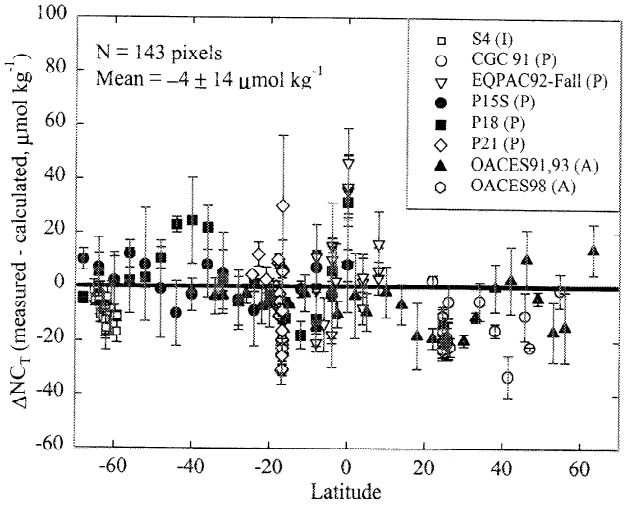

Figure 9. Comparison of C_T values calculated from pCO_{2SW} and A_T fields with the measured values (OACES 91, 93, and 98 for the Atlantic; CGC91, EQPAC 92 Fall, P21, P18, and P15S for the Pacific; S4I for the Indian section of the Southern Ocean). For comparison, the cruise data are binned into a 4° latitude × 5° longitude grid.

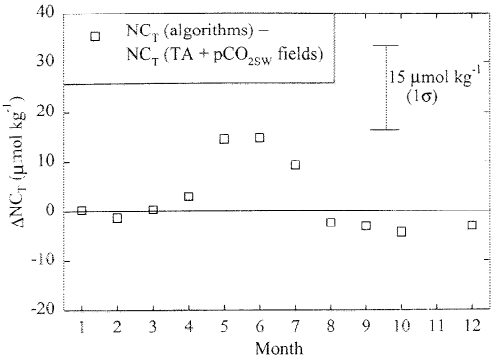

Figure 10. Comparison of estimated NC_T using the derived NC_T algorithms, NO_3^-, and SST with the calculated values from A_T – pCO_{2SW} fields for the western North Pacific (30°-60°N and 160°-180°E) where seasonal pCO_{2SW} data are available. Error bars represent standard deviations (1σ) of the differences for each month.

5. Conclusions

In low-latitude waters (30°S-30°N), the surface concentrations of NC_T show a minimum and are weakly correlated with SST except in the eastern equatorial Pacific where there is a much stronger anti-correlation with SST. At high latitudes (>30°), the NC_T increases with NO_3^- and is inversely proportional to SST. This increase in NC_T with decreasing temperature is attributed to the outcropping of subsurface waters rich in NC_T. The distribution of surface NC_T is derived by dividing the world's ocean into five regions with 12 equations relating NC_T to SST and NO_3^-. A parameterization of NC_T with SST and NO_3^- give reasonable estimates of overall regional trends and absolute concentrations. Error estimates derived from applying the derived algorithms to independent data and from comparing the estimated NC_T values using the derived algorithms with those calculated using A_T and pCO_{2SW} fields range up to ±15 μmol kg^{-1}. As new surface C_T, pCO_{2SW}, and A_T data become available in the future, it will be possible to improve the temporal and spatial resolutions of the global map of C_T.

Acknowledgments. The field work was jointly sponsored by the NOAA/OACES program and the DOE global CO_2 survey project and would not have been possible without the considerable effort of many scientists and crew members on the ships during the JGOFS, NOAA/OACES, DOE/WOCE, TTO, and SAVE expeditions collecting the data. The support by Lisa Dilling, NOAA/Global Carbon Cycle program manager, is greatly acknowledged. The authors would also like to thank Hee-Sook Kang of the Rosenstiel School of Marine and Atmospheric Science for preparing the color plates. Gail Derr prepared the camera-ready version of this text. This research was carried out, in part, under the auspices of the Cooperative Institute of Marine and Atmospheric Studies (CIMAS), a joint institute of the University of Miami and the National Oceanic and Atmospheric Administration, cooperative agreement NA67RJ0149.

References

Andrié C., C. Oudot, C. Genthon, and L. Merlivat, CO_2 fluxes in the tropical Atlantic during FOCAL cruises, *J. Geophys. Res., 91*, 11,741-11,755, 1986.

Bates, R.N., A.F. Michaels, and A.H. Knap, Seasonal and interannual variability of oceanic carbon dioxide species at the U.S. JGOFS

Bermuda Atlantic Time-series Study (BATS) site, *Deep Sea Res., Part II, 43,* 347-383, 1996.

Brewer, P.G., A. Brawshaw, and R. Williams, Measurements of total carbon dioxide and alkalinity in the North Atlantic Ocean in 1981, in *The Changing Carbon Cycle, A Global Analysis,* edited by J. Trabalka and D. Reichle, pp. 358-381, Springer-Verlag, New York, 1986.

Brewer, P.G., D.M. Glover, C. Goyet, and D.K. Shafer, The pH of the North Atlantic Ocean: Improvements to the global model for sound absorption in seawater, *J. Geophys. Res., 100,* 8761-8776, 1995.

Chen, C.-T., and R.M. Pytkowicz, On the total CO_2-titration alkalinity-oxygen system in the Pacific Ocean, *Nature, 281,* 362-365, 1979.

Chen, C.-T., F.J. Millero, and R.M. Pytkowicz, Comment on "Calculating the oceanic CO_2 increase: A need for caution" by A.M. Shiller, *J. Geophy. Res., 87,* 2083-2085, 1982.

Chen, C.-T., E.P. Jones, and K. Lin, Wintertime total carbon dioxide measurements in the Norwegian and Greenland Seas, *Deep Sea Res., Part I, 37,* 1455-1473, 1990.

Conkright, M.E., T.P. Boyer, and S. Levitus, Quality control and processing of historical nutrient data, *Tech. Rep. NESDIS 79,* Natl. Oceanic and Atmos. Admin., Silver Spring, Md., 1994.

Conway, T.J., P.P. Tans, L.S. Waterman, K.W. Thoning, D.R. Kitzis, K.A. Masarie, and N. Zhang, Evidence for interannual variability of the carbon cycle from the National Oceanic and Atmospheric Administration/Climate Monitoring and Diagnostics Laboratory global air sampling network, *J. Geophys. Res., 99,* 22,831-22,855, 1994.

Dickson, A.G., and F.J. Millero, A comparison of the equilibrium constants for the dissociation of carbonic acid in seawater media, *Deep Sea Res., Part I, 34,* 1733-1743, 1987.

Feely, R.A., R.H. Gammon, B.A. Taft, P.E. Pullen, L.S. Waterman, T.J. Conway, J.F. Gendron, and D.P. Wisegarver, Distribution of chemical tracers in the eastern equatorial Pacific during and after the 1982-83 El Niño/Southern Oscillation event, *J. Geophys. Res., 92,* 6545-6558, 1987.

Feely, R.A., R. Wanninkhof, C.E. Cosca, P.P. Murphy, M.F. Lamb, and M.D. Steckley, CO_2 distribution in the equatorial Pacific during the 1991-1992 ENSO event, *Deep Sea Res., Part II, 42,* 365-386, 1995.

Feely, R.A., R. Wanninkhof, C. Goyet, D.E. Archer, and T. Takahashi, Variability of CO_2 distributions and sea-air fluxes in the central and eastern equatorial Pacific during the 1991-94 El Niño, *Deep Sea Res., Part I, 44,* 1851-1867, 1997.

Feely, R.A., M.F. Roberts, D.J. Greeley, and R. Wanninkhof, Comparison of the carbon system parameters at the global CO_2 survey crossover locations in the North and South Pacific Ocean, 1990-1996, *ORNL-CDIAC-115,* 74 pp., Carbon Dioxide Inf. Anal. Cent., Oak Ridge Natl. Lab., Oak Ridge, Tenn., 1999a.

Feely, R.A., R. Wanninkhof, T. Takahashi, and P.P. Tans, The influence of equatorial Pacific CO_2 sea-air exchange on the growth rate of atmospheric CO_2, *Nature, 398,* 597-601, 1999b.

Goyet, C., and D. Davis, Estimation of total CO_2 concentration throughout the water column, *Deep Sea Res., Part I, 44,* 859-977, 1997.

Hoppema, J.M.J., E. Fahrbach, M. Schroder, A. Wisotski, and H.J.W. de Baar, Winter-summer differences of carbon dioxide and oxygen in the Weddell Sea surface layer, *Mar. Chem., 51,* 177-192, 1995.

Hoppema, J.M.J., E. Fahrbach, M.H.C. Stoll, and H.J.W. de Baar, Annual uptake of atmospheric CO_2 by the Weddell Sea derived from a surface layer balance, including estimations of entrainment and new production, *J. Mar. Syst., 19,* 219-233, 1999.

Inoue, H.Y., H. Matsueda, M. Ishii, K. Fushimi, M. Hirota, I. Asanuma, and Y. Takasugi, Long-term trend of the partial pressure of carbon dioxide (pCO_2) in surface waters of the western North Pacific, 1984-1993, *Tellus, Ser. B, 47,* 391-413, 1995.

Johnson, K.M., P.J.leB. Williams, L. Brändström, and J.M. Sieburth, Coulometric TCO_2 analysis for marine studies: Automation and calibration, *Mar. Chem., 21,* 117-133, 1987.

Johnson, K.M., K.D. Wills, D.B. Butler, W.K. Johnson, and C.S. Wong, Coulometric total carbon dioxide analysis for marine studies: Maximizing the performance of an automated gas extraction system and coulometric detector, *Mar. Chem., 44,* 167-187, 1993.

Kalnay, E., et al., The NCEP/NCAR 40-year reanalysis project, *Bull. Am. Meteorol. Soc., 77,* 437-471, 1996.

Keeling, C.D., Carbon dioxide in surface ocean waters, 4, Global distribution, *J. Geophys. Res., 73,* 4543-4553, 1968.

Keeling, R.F., R.P. Najjar, M.L. Bender, and P.P. Tans, What atmospheric oxygen measurements can tell us about the global carbon cycle, *Global Biogeochem. Cycles, 7,* 37-67, 1993.

Lee, K., F.J. Millero, and R. Wanninkhof, The carbon dioxide system in the Atlantic Ocean, *J. Geophys. Res., 102,* 15,693-15,707, 1997.

Levitus, S., R. Burgett, and T.P. Boyer, *World Ocean Atlas 1994,* vol. 3, *Salinity, NOAA Atlas, NESDIS, 3,* 97 pp., Natl. Oceanic and Atmos. Admin., Silver Spring, Md., 1994.

Mehrbach, C., C.H. Culberson, J.E. Hawley, and R.M. Pytkowicz, Measurements of the apparent dissociation constants of carbonic acid in seawater at atmospheric pressure, *Limnol. Oceanogr., 18,* 897-907, 1973.

Millero, F.J., K. Lee, and M. Roche, Distribution of alkalinity in the surface waters of the major oceans, *Mar. Chem., 60,* 111-130, 1998.

Murphy, P.P., K.C. Kelly, R.A. Feely, and R.H. Gammon, Carbon dioxide concentrations in surface water and the atmosphere during 1986-1989 PMEL cruises in the Pacific and Indian Oceans, *ORNL-CDIAC-75 NDP-047,* Carbon Dioxide Inf. Anal. Cent., Oak Ridge Natl. Lab., Oak Ridge, Tenn., 1995.

Murray, J.W., R.T. Barber, M.R. Roman, M.P. Bacon, and R.A. Feely, Physical and biological controls on carbon cycling in the equatorial Pacific, *Science, 266,* 58-65, 1994.

Oceanographic Data Facility (ODF), South Atlantic Ventilation Experiment (SAVE) chemical, physical, and CTD data report, Legs 1, 2, and 3, *SIO ref. 92-9,* La Jolla, Calif., 1992a.

Oceanographic Data Facility (ODF), South Atlantic Ventilation Experiment (SAVE) chemical, physical, and CTD data report, Legs 4 and 5, *SIO ref. 92-10,* La Jolla, Calif., 1992b.

Physical and Chemical Oceanographic Data Facility (PCODF), Transient Tracers in the Ocean/North Atlantic Study (TTO/NAS), Shipboard physical and chemical data report, *SIO ref. 86-15,* La Jolla, Calif., 1986a.

Physical and Chemical Oceanographic Data Facility (PCODF), Transient Tracers in the Ocean/Tropical Atlantic Study (TTO/TAS), Shipboard physical and chemical data report, *SIO ref. 86-16,* La Jolla, Calif., 1986b.

Poisson, A., and C.-T. Chen, Why is there little anthropogenic CO_2 in the Antarctic Bottom Water?, *Deep Sea Res., Part I, 34,* 1255-1275, 1987.

Poisson, A., N. Metzl, C. Brunet, B. Schauer, B. Bres, D. Ruiz-Pino, and F. Louanchi, Variability of sources and sinks of CO_2 in the western Indian and Southern Oceans during the year 1991, *J. Geophys. Res., 98,* 22,759-22,778, 1993.

Takahashi, T.T., W.S. Broecker, and S.R. Werner, Isotope marine chemistry, pp. 291-326, Geoch. Res. Assoc., Tokyo, Japan, 1980.

Takahashi, T.T., D.W. Chipman, and T. Volk, Geographical, seasonal, and secular variations of the partial pressure of CO_2 in surface waters of the North Atlantic Ocean: The results of the North Atlantic TTO Program, in *Carbon Dioxide, Science and Consensus (CONF-820970),* pp. 123-145, Oak Ridge Assoc. Univ., Inst. for Energy Anal., Oak Ridge, Tenn., 1983.

Takahashi, T., J. Olafsson, J.G. Goddard, D.W. Chipman, and S.C. Southerland, Seasonal variation of CO_2 and nutrients in the high-latitude surface oceans: A comparative study, *Global Biogeochem. Cycles, 7,* 843-878, 1993.

Takahashi, T., R.A. Feely, R.F. Weiss, R. Wanninkhof, D.W. Chipman, S.C. Sutherland, and T. Takahashi, Global air-sea flux of CO_2: An estimate based on measurements of sea-air pCO_2 difference, *Proc. Natl. Acad. Sci. U.S.A., 94,* 8292-8299, 1997.

Tans, P.P., I.Y. Fung, and T. Takahashi, Observational constraints on the global atmospheric CO_2 budget, *Science, 247,* 1431-1438, 1990.

Wanninkhof, R., and R.A. Feely, fCO_2 dynamics in the Atlantic, South Pacific, and South Indian Oceans, *Mar. Chem., 60,* 15-31, 1998.

Winguth, A.M.E., M. Heimann, K.D. Kurz, E. Maier-Reimer, U. Mikolajewicz, and J. Segschneider, El Niño-Southern Oscillation related fluctuations of the marine carbon cycle, *Global Biogeochem. Cycles, 8,* 39-63, 1994.

Winn, C.D., Y.-H. Li, F.T. Mackenzie, and D.M. Karl, Rising surface ocean dissolved inorganic carbon at the Hawaii Ocean Time-series site, *Mar. Chem., 60,* 33-47, 1998.

Wong C.S., and Y.-H. Chan, Temporal variations in the partial pressure and flux of CO_2 at ocean station P in the subarctic northeast Pacific Ocean, *Tellus, Ser. B, 43,* 206-223, 1991.

R.A. Feely, Pacific Marine Environmental Laboratory, NOAA, 7600 Sand Point Way, N.E., Seattle, WA 98115.

K. Lee, T.-H. Peng, and R. Wanninkhof, Atlantic Oceanographic and Meteorological Laboratory, NOAA, Ocean Chemistry Division, 4301 Rickenbacker Causeway, Miami, FL 33149 (lee@aoml.noaa.gov).

F. Millero, Rosenstiel School of Marine and Atmospheric Science, MAC, University of Miami, 4600 Rickenbacker Causeway, Miami, FL 33149.

(Received September 15, 1998; revised February 16, 2000; accepted February 21, 2000.)